Research Article | Vol. 28, No. 18 / 31 August 2020 / Optics Express 27013
Optics EXPRESS

# Mid-IR sensing platform for trace analysis in aqueous solutions based on a germanium-on-silicon waveguide chip with a mesoporous silica coating for analyte enrichment

NURIA TEIGELL BENÉITEZ,[1,*] BETTINA BAUMGARTNER,[2] JEROEN MISSINNE,[3] SANJA RADOSAVLJEVIC,[1] DOMINIK WACHT,[2] STEFAN HUGGER,[4] PAWEŁ LESZCZ,[5] BERNARD LENDL,[2] AND GUNTHER ROELKENS[1]

[1]*Photonics Research Group, INTEC, Ghent University-imec, Technologiepark 126, 9052, Belgium*
[2]*Research Division of Environmental Analytics, Process Analytics and Sensors, Institute of Chemical Technologies and Analytics, Technische Universität Wien, Getreidemarkt 9, 1060 Vienna, Austria*
[3]*CMST, ELIS, Ghent University-imec, Technologiepark 126, 9052, Belgium*
[4]*Fraunhofer Institute for Applied Solid State Physics, Tullastrasse 72, 79108 Freiburg, Germany*
[5]*VigoSystem S.A. Poznańska street 129/133 05-850 Ożarów Mazowiecki, Poland*
[*]*nuria.teigellbeneitez@ugent.be*

**Abstract:** A novel platform based on evanescent wave sensing in the 6.5 to 7.5 µm wavelength range is presented with the example of toluene detection in an aqueous solution. The overall sensing platform consists of a germanium-on-silicon waveguide with a functionalized mesoporous silica cladding and integrated microlenses for alignment-tolerant back-side optical interfacing with a tunable laser spectrometer. Hydrophobic functionalization of the mesoporous cladding allows enrichment of apolar analyte molecules and prevents strong interaction of water with the evanescent wave. The sensing performance was evaluated for aqueous toluene standards resulting in a limit of detection of 7 ppm. Recorded adsorption/desorption profiles followed Freundlich adsorption isotherms with rapid equilibration and resulting sensor response times of a few seconds. This indicates that continuous monitoring of contaminants in water is possible. A significant increase in LOD can be expected by likely improvements to the spectrometer noise floor which, expressed as a relative standard deviation of 100% lines, is currently in the range of $10^{-2}$A.U.



## 1. Introduction

Water is not only essential for all forms of life but also it is used in nearly every industrial process. To assure a safe environment, novel water monitoring technologies are needed for all types of water including process water, wastewater as well as drinking water. In particular organic contaminants are one of the major pollutants of water [1] and their detection concerns the identification of a complex mixture of many different molecules. In this regard, mid-infrared (mid-IR) spectroscopy has proven to be a very suitable sensing method since it provides direct information on the molecular fingerprint of the analytes [2–3]. For detecting hydrocarbons in water established mid-IR spectroscopic methods required the use of chlorofluorocarbons (CFCs) extraction solvent in a liquid-liquid extraction step followed by transmission measurement in a dedicated flow cell. As CFCs have been banned by international regulations [4], these analyses are nowadays mainly based on an extraction step employing defined aliphatic hydrocarbons followed by selective gas chromatography or gravimetry after solvent evaporation [5]. These methods rely

#399646 https://doi.org/10.1364/OE.399646
Journal © 2020 Received 8 Jun 2020; revised 24 Jul 2020; accepted 25 Jul 2020; published 28 Aug 2020

Optics EXPRESS

on manual operation and they currently have to be performed in dedicated laboratories, which is labor and cost intensive as well as time consuming [6]. Thus, there is a clear drive for the development of solutions allowing for a reliable and continuous real-time monitoring of water on site. In this paper we propose a chip-based approach in the form of disposable sensor chips which can be exchanged by non-expert operators. The sensor chip consists of a germanium-on-silicon (GOS) optical waveguide covered with a functionalized mesoporous silica coating. Instead of separating the target analytes from the aqueous phase by means of a liquid-liquid extraction step, apolar analytes are enriched in the mesoporous coating of the sensor chip and thus also separated from the aqueous phase, which then only negligibly interacts with the evanescent field. Quantum cascade laser (QCL) light is coupled from the chip back-side into the waveguide making use of grating couplers and monolithically integrated microlenses. By this means a limit of detection (LOD) for aromatic hydrocarbons sufficiently low to meet the regulation requirements (~1 ppm for industry, sub-ppm for drinking water) [7,8] can be reached. Here first measurements of toluene in water reveal a detection limit of 7 ppm, limited by the noise of the used laser spectrometer.

## 2. Chip-based evanescent wave sensing platform

The developed chip-based evanescent wave sensing platform relies on obtaining an absorption spectrum as a result of the interaction of an evanescent field with the target molecules. For this platform, the mid-IR wavelength range between 6.5 -7.5 µm was selected, where molecules have a strong fingerprint absorption spectrum [9–11]. This approach enables sensitive, quantitative and selective detection of a wide range of molecules directly in a water stream (in-line detection). To the best of our knowledge, the state-of-the-art for on-chip absorption spectroscopy in CMOS-compatible long-wave mid-infrared platforms is limited to a few reported proofs-of concept [11–18] showing the potential for sensing, but until today there are no reports on the detection of ppm-concentrations of an analyte neither in gas phase nor in liquid phase. Compared to a standard attenuated total internal reflection (ATR) unit were the evanescent field is interacting with the analyte at a limited number of locations in an ATR crystal [19], the use of waveguides can enhance the sensitivity by increasing the effective interaction length [1,20,21]. However, the requirements on LOD and the strong absorption of the aqueous matrix in the mid-infrared prevents the use of water-clad waveguide structures for sensing. An elegant solution consists in cladding the waveguides with a hydrophobic layer that can enrich the targeted analyte and exclude the strong IR-absorber water to interact with the evanescent field. The coating can reversibly absorb or adsorb and in either case accumulate the analytes of interest, resulting in concentration enhancement factors in the range of 200-900 depending on the analyte [22–23] which are very high and do not require the use of solvents for analyte extraction [16,17] . When using polymer coatings for analyte enrichment response times are slow, typically requiring several tens of minutes upon responding to a change in analyte concentration as analyte molecules need to dissolve in the solid polymer and diffuse toward the evanescent field extending from the ATR surface. Introduction of surface modified mesoporous coatings, where the enrichment process proceeds via an adsorption process described by Freundlich or Langmuir adsorption isotherms, is much faster with enrichment times down to a few seconds, eventually making them suitable for continuous monitoring [20]. In contrast to using polymer coatings, surface modification in mesoporous films also allows to adjust the selectivity as required. This concept has been recently demonstrated on ATR crystals using functionalized mesoporous silica coatings for detecting benzonitrile and valeronitrile as examples for apolar molecules, as well as nitrate as an example for a polar analyte in water [23,24]. Furthermore, again employing miniaturized multi-bounce ATR crystals, expansion of this concept to gas sensing of aromatic hydrocarbons has been shown too [24]. In this work we employ modified mesoporous silica for the first time on a Germanium-on-Silicon (GOS) waveguide.

Optics EXPRESS

The proposed system is illustrated in Fig. 1 and consists of a GOS waveguide cladded with a dedicated mesoporous silica coating which is in contact with the water stream to be monitored. The chip architecture requires broadband optical coupling interfacing with the chip from the back side. This is achieved by developing novel grating coupler structures in combination with monolithically integrated back-side microlenses. Furthermore, this microlens-based optical interface drastically increases the alignment tolerance between the passive chip and the read-out unit (QCL and detector) by implementing the expanded beam concept [25], so it allows easy and fast chip replacement. Since the lenses are monolithically integrated on the chip back-side, the fabrication concept is also compatible with wafer-scale fabrication, reducing the cost. This coupling concept was demonstrated for first time in the NIR (1330 nm) using polymer microlenses [26–27] and afterwards using Si microlenses in the C-band [28] and here it is applied for expanded beam coupling in the targeted 6.5 µm-7.5 µm wavelength range.

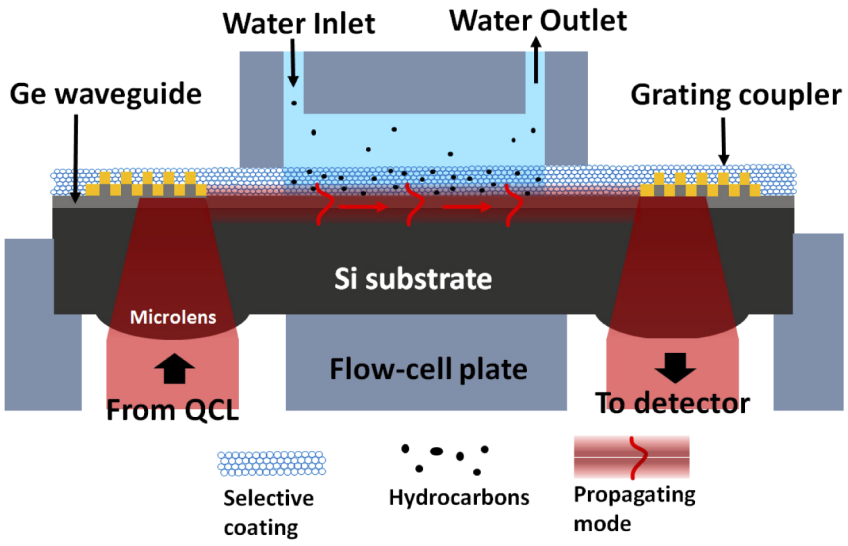


**Fig. 1.** Schematic illustrating the working principle of the sensor. The sensor consists of a germanium-on-silicon optical waveguide covered with a functionalized mesoporous silica coating. Quantum cascade laser (QCL) light is coupled from the chip back-side into the waveguide making use of grating couplers and monolithically integrated microlenses.

## 3. Integrated circuit platform and sensor chip design

The sensor chip was realized on the germanium-on-silicon (GOS) platform consisting of a 2 µm thick Ge waveguide layer to ensure single mode waveguiding at a wavelength of 6.5 µm while minimizing the mode confinement in the interlayer between Ge and Si, which has been identified to be one of the major causes of propagation loss [18,29,30]. The Ge layer was partially (1 µm) etched to achieve grating couplers and rib waveguides (waveguide width of 3.3 µm for single-mode operation) in one etch step. Furthermore, this partial etch reduces the surface topography thereby facilitating the integration of the mesoporous silica coating.

A 16 mm long straight waveguide was used having an input and output grating coupler on each side (see Fig. 1). Both grating couplers are identical, were designed for nearly vertical incidence angles and consist of 8 periods, 1 µm etched with 50% duty cycle, achieving strong diffraction. Directly on top of the Ge grating, gold was deposited to improve the downward directionality, as shown in Fig. 2(A). Below the grating coupler, on the back side of the chip, a microlens was etched into the silicon substrate which was designed to focus a 130 µm diameter collimated

Optics EXPRESS

external beam onto the grating coupler (and conversely to collimate the light emitted by the output grating). This 130 μm beam diameter was chosen to obtain a sufficiently large Rayleigh range for free space optics systems. The use of microlenses not only serves as a focusing and collimating element but implements an expanded beam interface, which drastically increases the lateral alignment tolerance between the chip and the readout unit [25–28].

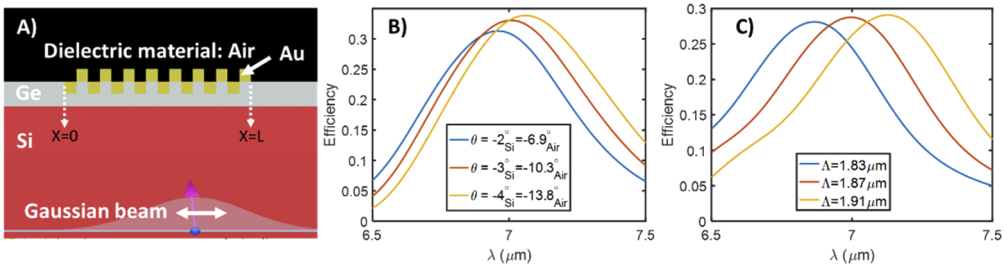


**Fig. 2.** (A) a cross-section of the grating structure for a beam located at X/L=0.7, where L is the total length of the grating and a negative incidence angle. The data presented corresponds to a mode travelling to the right; (B) coupling spectra (Λ=1.83 μm) as a function of in-coupling angle; (C) coupling spectra ($\theta_{Si} = 0°$) as a function of grating period. TE polarization was assumed in these simulations

The grating was designed to ensure sufficient coupling efficiency over the full targeted wavelength range (6.5-7.5 μm, TE polarization) under close to normal incidence to facilitate the interfacing with the readout unit. Figures 2(B) and (C) shows typical simulated coupling spectra at various angles of incidence (Λ=1.83 μm) and for varying grating pitch Λ ($\theta_{Si}$=0°). A Gaussian beam waist of 7.5 μm is used in the simulation. A large bandwidth (~600 nm 3dB BW) was obtained, as compared to other grating couplers in similar platforms [18,31,32]. This comes at the expense of a reduced peak efficiency (~30%) and increased back-reflection (~20%). The simulated total interfacing coupling spectrum (i.e. in- and out-coupling) for a grating pitch of 1.87 μm is shown in Fig. 3(A). Since in the system the detector collects all the light received by the out-coupling microlens, the total efficiency was obtained by multiplying the laser-to-chip in-coupling efficiency by the total power directed towards the substrate (~70%) when the propagating mode interacts with the outcoupling grating.

The intrinsic grating coupler tolerance to misalignments (i.e. without taking in account the effect of microlenses) was estimated through simulations by sweeping the beam incidence position (see Fig. 3(B)) and a 1 dB alignment tolerance of ± 2.75 μm was found. In order to improve the alignment tolerance, an expanded beam concept was used by integrating microlenses on the back-side of the chip surface.

A model for the lens system was implemented in Zemax OpticStudio (Fig. 4) and fine-tuned using the Gaussian beam propagation method for an operating wavelength of 7 μm and an angle of incidence near 0°. The design was optimized so that an external 130 μm diameter collimated beam is focused onto the grating coupler, with a beam waist of 7.5 μm, which requires a lens focal distance equal to the chip thickness. This results in a Si lens radius of curvature (ROC) of 538 μm (250 μm lens diameter) for a 750 μm thick chip. The design is also relatively tolerant for variations in the ROC, as shown in Fig. 4, which relaxes requirements on the fabrication process.

When sweeping the lateral position of the external beam with respect to the microlens, a 1 dB tolerance of ± 30 μm was found, significantly larger than the intrinsic alignment tolerance of the grating coupler (± 2.75 μm). It should be noted that when the 130 μm input beam gets laterally misaligned with respect to the ideal position on the lens, the lens will deviate the beam onto the grating coupler under a different angle of incidence. This angle change may additionally lead to a change in coupling efficiency, depending on the grating angular dependence, which is

Optics EXPRESS

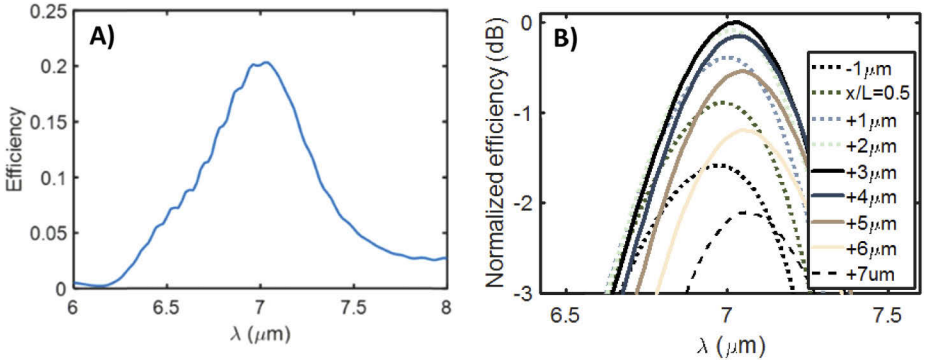


**Fig. 3.** (A) simulated optical interfacing (in- and out- coupling) efficiency for a grating pitch of 1.87 µm; (B) simulated impact of the position of the incident beam at the grating on the coupling efficiency. The position origin is the middle of the grating (x/L=0.5). From there positive sign indicates the direction towards the waveguide. We can see that the optimum coupling position is at +3 µm from the center and a 1 dB tolerance of ± 2.75 µm is obtained (from X=0.5L to x=0.5L+5.5 µm).

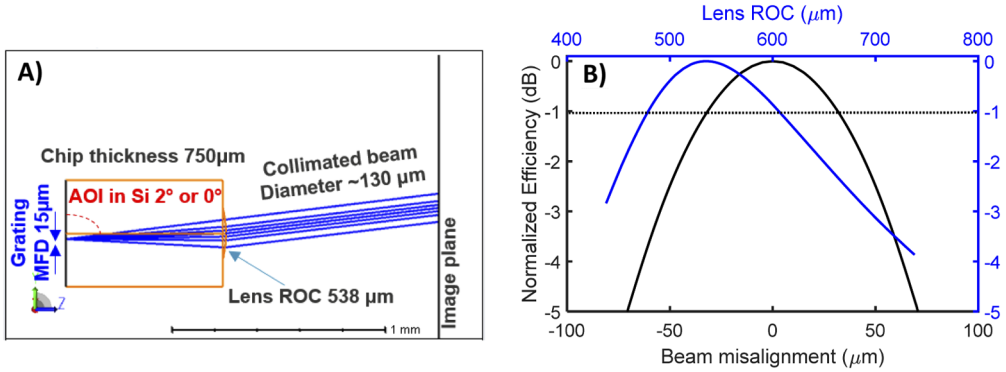


**Fig. 4.** (A) Micro-lens model implemented in Zemax OpticStudio. (B) Simulated normalized coupling efficiency of the lens system as a function of lateral beam misalignment and as a function of lens ROC.

not taken into account in this model, but for the designed gratings, this dependence is low (see Fig. 2) and can therefore in first order be neglected. However, it should be mentioned that, due to the Gaussian beam propagation method used for the lens design, it was assumed that the grating coupler emits/accepts a Gaussian mode, which is clearly an approximation.

One of the drawbacks of the expanded beam concept is that the increased lateral alignment tolerance comes at the expense of a decreased angular tolerance of positioning the chip with respect to the reader. However, when using an appropriate chip holder (see below), angular misalignments between chip and readout unit can much more easily be dealt with than lateral misalignments.

For the demonstration of the sensing principle, an array of straight trenched waveguides (see Fig. 5(A)) was realized with variations in grating pitch (from 1.73 µm to 1.91 µm) in order to compensate deviations during fabrication (e.g. duty cycle, lens position deviation) and testing (e.g. in coupling angle). Also, given the number of possible variations that fitted in the sample, larger pitch variations than required were included for enabling the testing of different substances using the same chips. The distance between the in- and outcoupling grating was set at 16 mm.

Optics EXPRESS

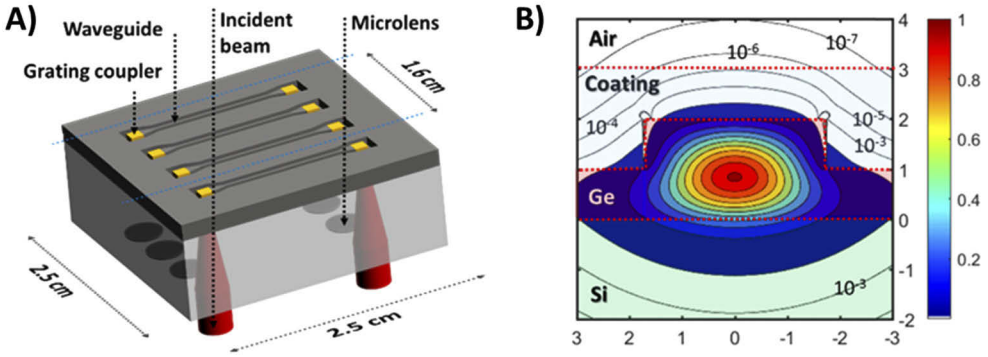


**Fig. 5.** (A) the design of the fabricated chip showing the chip configuration and interfacing approach; QCL light (red) is coupled from the backside; (B) waveguide cross section and overlapped normalized mode intensity distribution at 6.7 μm. This configuration results in a confinement factor in the coating of 1.1%.

The Ge rib waveguides were implemented by etching a pair of trenches defining the waveguide core as the space between them. The width of these trenches (8 μm) was selected to ensure no leakage of the propagating mode while keeping them narrow. The idea behind the trenched approach is that this approach will facilitate the conformal deposition of a sufficiently thick mesoporous silica coating, as discussed below. The targeted thickness of the coating on top of the waveguides was 1 μm. This choice was made as a compromise between having sufficient isolation of the optical mode from the water and allowing a penetration of the target analyte to the waveguide surface [21].

The coating refractive index was modeled using the Bruggeman Effective Medium Approximation (BEMA) for the effective dielectric permeability of a binary mixture [33] and assuming a porosity of 50%, corresponding to the data obtained in previous characterization of these coatings [34]. The simulated confinement factor and loss in the coating ranges from ~1.0% and 0.6dB/cm ($\lambda$=6.5 μm, n=1.1) to ~1.4% to 3.6dB/cm ($\lambda$=7.5 μm, n=0.97) for TE polarization.

## 4. Sensor chip fabrication

The sensor chip fabrication can be divided in three main steps: fabrication of the waveguides with grating couplers, fabrication of the microlenses on the back side and deposition of the mesoporous enrichment coating as a top cladding on the Ge waveguide. Figure 6 illustrates the fabrication process flow.

Cleaved sample-size pieces taken from a GOS 4 inch wafer were used for fabricating individual sensor chips. The waveguides, gratings and aligning marks are defined by means of UV contact lithography using MIR701 photoresist as a soft mask. Then, the defined pattern is transferred into the Ge layer through reactive ion etching (RIE) with a mixture of CF4, SF6 and H2. After etching, the remaining resist mask is first cleaned by rinsing in acetone, IPA and DI water and then using an oxygen plasma. The achieved waveguide quality is illustrated in Fig. 7(A). The Au top cladding on the grating couplers is defined through lift-off of a 1 μm Au coating through e-gun evaporation. A cross-section of the grating coupler structure is shown in Fig. 7(B). To ensure chemical compatibility of the photonic integrated circuit with the mesoporous coating deposition, a thin (~20 nm) $SiO_x$ layer was deposited on the surface using plasma-enhanced chemical vapor deposition (PECVD).

Then, for realizing the microlenses, in a first step, the top side of the chip having the optical structures was protected with a thick layer of photoresist. Subsequently, the back side of the chip (750 μm thick) was polished to achieve an optically smooth surface. Afterwards, photoresist

Optics EXPRESS

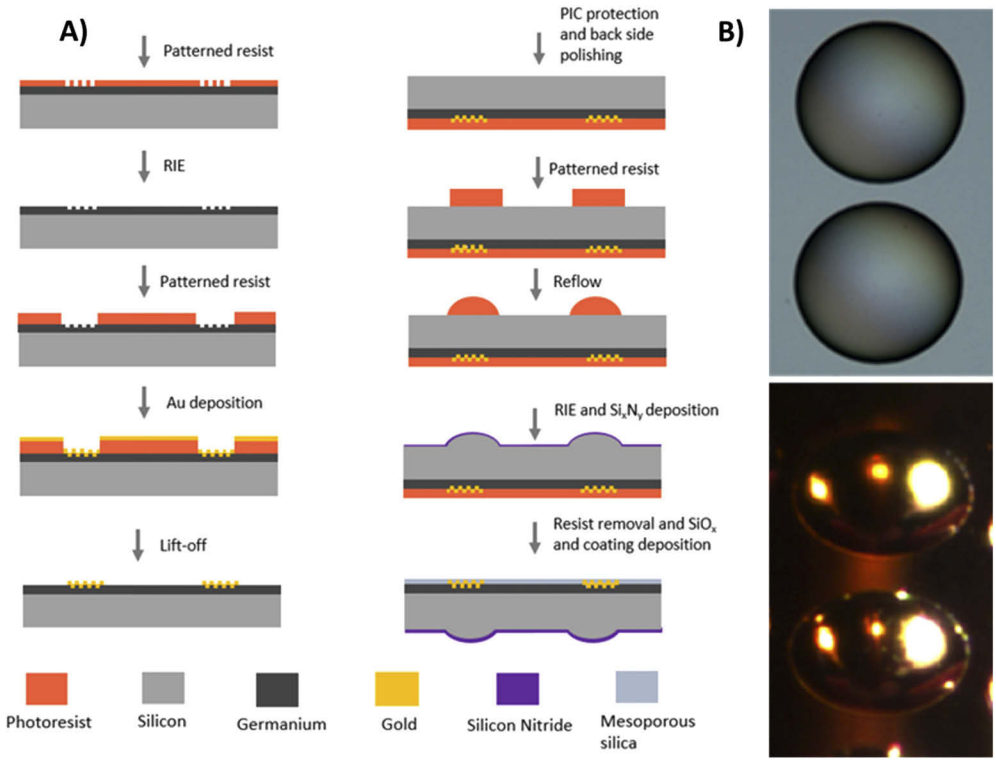


**Fig. 6.** (A) fabrication flow for realizing the chips with mesoporous coating and back-side monolithically integrated microlenses; (B) microscope pictures with a view on the back-side microlenses

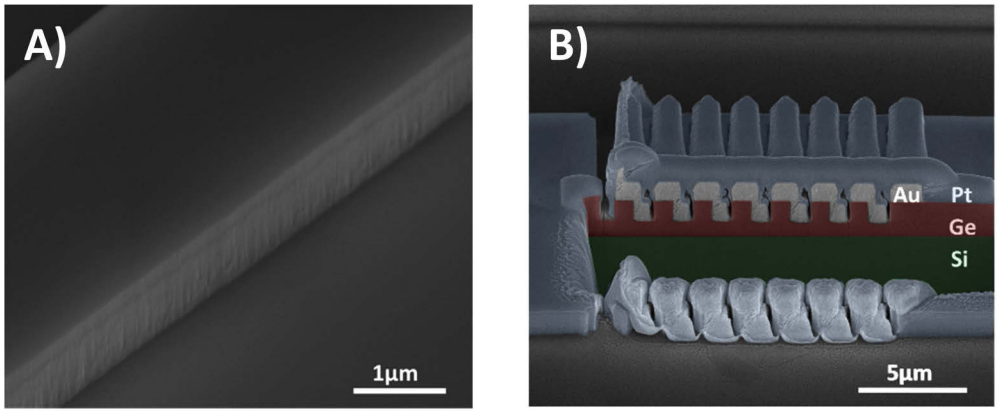


**Fig. 7.** (A) SEM micrograph of a single mode germanium-on-silicon waveguide. The measured width in the single-mode region was 3.4µm; (B) cross-section of the grating coupler with Au top cladding. A platinum layer was deposited in the cross-section location to protect the structures before FIB cross-section preparation.

Optics EXPRESS

(AZ4562,12 µm thick) was applied on the back side of the chip and it was patterned using UV-lithography (EVG 620 double-sided mask aligner) so that only resist cylinders with a diameter of 250 µm remain at the location where lenses are required. Then, these photoresist structures are reflown on a hotplate at 150°C and as a result, the photoresist cylinders are transformed into nearly spherical microlenses Finally, the photoresist lenses are transferred into the Si substrate using RIE ($SF_6$:$O_2$) and a 900 nm thick $Si_xN_y$ anti-reflection coating was deposited on the etched lenses by means of PECVD deposition.

The synthesis and deposition of the mesoporous 3D hexagonal structured coating is based on the evaporation-induced self-assembly process using cetyltrimethylammonium bromide (CTAB) as template and was performed analogous to our previous report [22]. 3 layers were spin-coated on top of each other with a thermal treatment at 110 °C over night between each deposition. After deposition of the layers, the surface modification was performed using hexamethyldisilazane in absolute acetone. Thereby, mesoporous silica films with a water contact angle of 85°, a pore size of 3.7 nm and porosity of 50% were obtained [22,34]. Figure 8 shows the cross section of the waveguides covered with a 1 µm thick coating. Note that the silica cladding is homogeneous, and no isolated layers are visible. A top view SEM micrograph illustrates that the coating surface is smooth and free of defects (Fig. 8(B)).

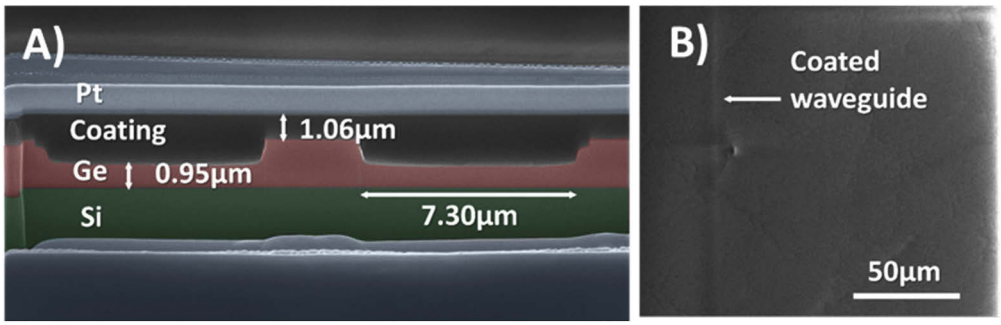


**Fig. 8.** FIB cross-section (A) and top view (B) of coated chips with trenched waveguides. A platinum layer was deposited in the cross-section location to protect the structures before FIB cross-sectioning.

## 5. Experiments

### *5.1. 2 µm GOS platform propagation loss and grating coupling tolerance/bandwidth*

The propagation loss of air-clad 3.3 µm wide partially etched GOS waveguides was evaluated using an in-house setup consisting of a similar quantum cascade laser source (6.7-7.45 µm tuning range) and detector as used in the spectrometer (see section 5.2). The QCL emission was coupled to an AsSe single mode microstructured fiber (SelenOptics, SM [35]) and then butt-coupled to cleaved facet waveguides of different lengths. The waveguide propagation loss is shown in Fig. 9(A). Overall, a propagation loss lower than ~5 dB/cm was measured over the whole wavelength range, which is in line with the values reported for similar platforms [9,18,29].

The tolerance with respect to the in-coupling position of a 130 µm wide beam was evaluated using an in-house setup as well. Hollow-core fibers (Opto-Knowledge Systems, Inc, SM, ID=200 µm [36]) providing a Gaussian beam of 130 µm diameter were used to couple light to and from the in- and out-coupling microlenses respectively. In steps of 5 µm, the position of the in-coupling fiber was varied for the directions parallel and perpendicular to the grating lines. For both directions, the estimated 1 dB excess loss alignment tolerance was found to be ±10 µm, as shown in Fig. 9(B), which is ~4 times greater than the simulated alignment tolerance in the y-direction

Optics EXPRESS

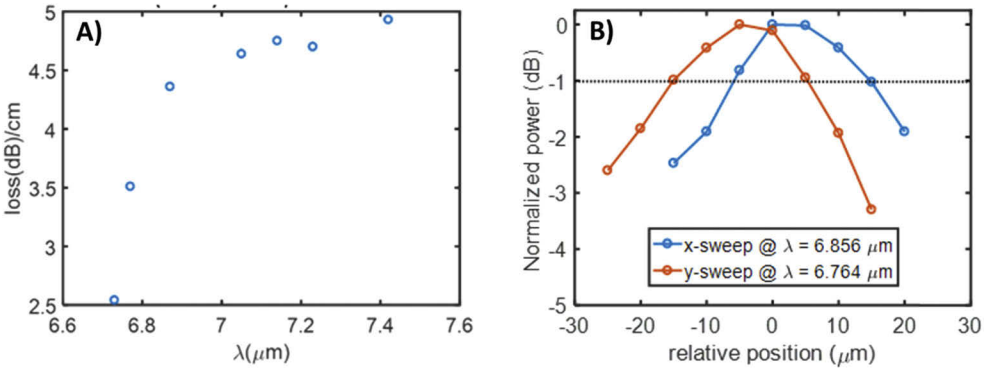


**Fig. 9.** (A) waveguide propagation losses in the 6.7-7.45 μm wavelength range; (B) Tolerance to misalignment in the directions perpendicular (x) and parallel (y) to the in-coupling direction.

at the grating without the microlens as shown in Fig. 3(B). However, this result is ~3 times worse than that obtained in simulations (±30 μm). We believe that the main reason for this mismatch is because the simulation program relies on Gaussian beam theory, which is valid only under paraxial approximation i.e. when the beam radius at the waist is much larger than the wavelength. In our case, the beam radius is ~7.5 μm, and deviations from the model are expected.

Sensing chips as described in section 3 were tested prior to and after mesoporous coating deposition, using the spectrometer described in section 5.2. The detected power spectrum is shown in Fig. 10, together with the QCL output power spectrum. This is the result of the incoupling and outcoupling gratings as well as the propagation through 1.6 cm of waveguide. The measured 3 dB bandwidth of ~500 nm is in agreement with the simulated values (Fig. 3(A)) and a factor ~3-5 times greater than those reported for similar platforms [18,31,32].

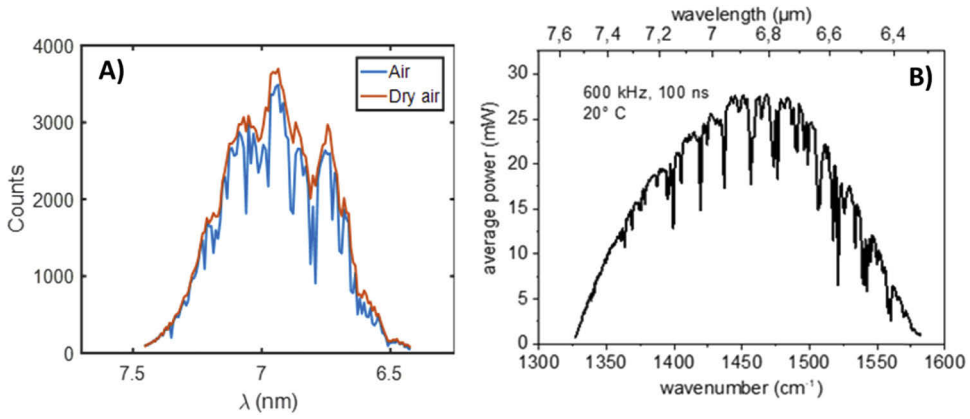


**Fig. 10.** (A) spectra recorded using the spectrometer for 1.6cm waveguides interfaced with downward grating couplers and microlenses under air and dry air environments; (B) QCL power spectrum measured in air prior to be mounted in the spectrometer.

Optics EXPRESS

### 5.2. Tunable laser spectrometer

The sensing experiments were carried out with a prototype of a compact tunable laser spectrometer (TLS) developed in the H2020 project AQUARIUS. The light source is a micro-opto-electro-mechanical system external cavity quantum cascade laser (MOEMS EC-QCL) module with an output power spectrum shown in Fig. 10(B) (600 kHz pulse repetition rate, 100 ns pulse length). The used detector was a HgCdTe high speed detector integrated with a low-noise preamplifier, TEC controller and data acquisition and processing unit. The detectivity of the detector was $D^* \geq 4.0 \times 10^9$ cm·$\sqrt{\text{Hz}}$/W.

An add-on unit for optical and chemical interfacing of the sensor chip was implemented in front of the spectrometer, as illustrated in Fig. 11. This add-on unit converts the 8 cm input-output beam spacing of the spectrometer into a 16 mm input-output spacing on the sensor chip and

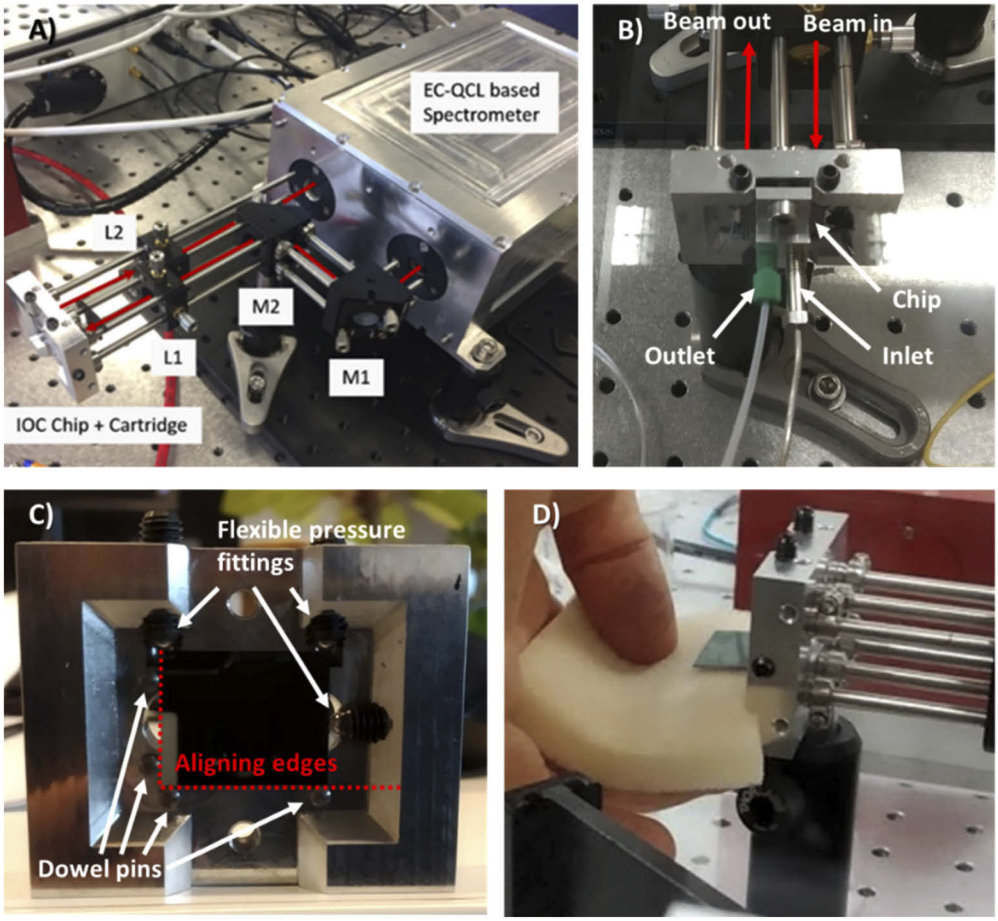


**Fig. 11.** a) illustration of the measurement setup. The add-on unit for chemical and optical interfacing consists of the flow-cell sample holder, two mirrors (M1, M2) and two lenses (L1,L2). b) close-up of the attached flow-cell sample holder. c) Chip inserted in the bottom plate of the flow cell with the positioning elements (flexible pressure fittings and dowel pins) and d) the manual replacement of a chip by mounting it in the bottom plate of the flow-cell using a sponge to protect the chip. After chip placement, the beam position on the chip substrate was selected by actuating L1 in order to have sufficient power in the spectral region of interest.

Optics EXPRESS

converts between the QCL output beam diameter of 3 mm and the required 130 µm beam diameter for interfacing with the microlenses on the back side of the chip. The sensor chips are mounted on a flow-cell plate using 3 dowel pins and 3 flexible pressure fittings and the flow cell is then attached using 2 screws to bring an FKM o-ring in contact with the surface of the chip. The waveguide length inside the o-ring is 8 mm, defining the interaction length.

After manual positioning of the chip into the flow cell, the position of the beam incident on the sample substrate was modified using M1 and L1 (See Fig. 11(A) and Fig. 12(A)). Actuating L1 in vertical direction allowed to select different waveguides on the chip (Fig. 5(A)). The tolerance of the system for chip replacement was assessed by adjusting the chip output signal to maximum, and subsequently removing the reference chip 10 times without changing any lens or mirror and evaluating the change of the recorded power. The variation of the total insertion loss, as shown in Fig. 12, is within 1 dB. If we compare these values with the measurements on tolerance in misalignment performed using the hollow core fibers as explained above, this corresponds to a misalignment of ~10 µm. This value correlates well with the placement accuracy expected from the alignment mechanism. This result indicates that the design is well suited for fast and easy chip replacement.

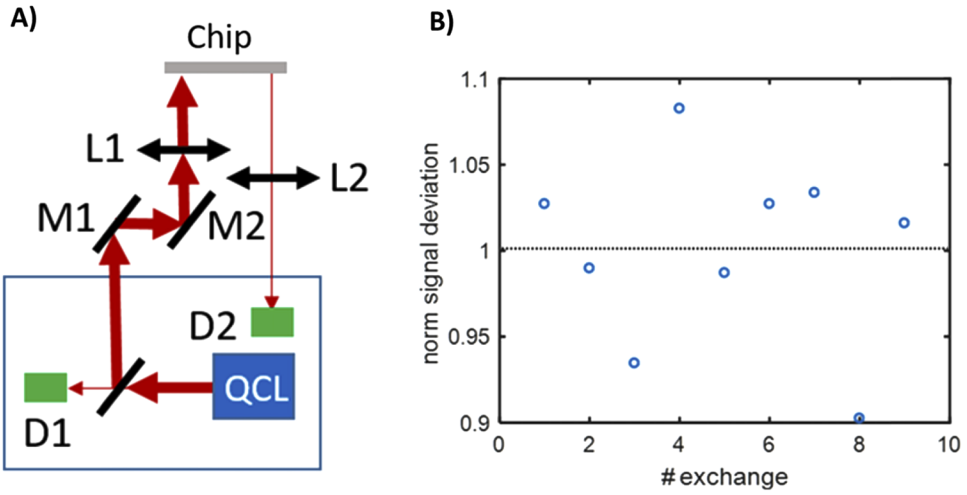


**Fig. 12.** (A) Schematic illustrating the optical path from the QCL to the reference detector (D1) and output detector (D2). The light is guided using mirrors (M1, M2) and the beam focused on the chip and detector (D2) using lenses (L1, L2) ; (B) Normalized signal deviation at 1392 $cm^{-1}$ (~7.18 um) between each chip exchange.

### *5.3. Sensing performance: toluene in water*

For the sensing measurements, a liquid flow cell was used in combination with a stainless steel tubing in the inlet (see Fig. 11(b)). A peristaltic pump was used to set the flow of the reference and sample liquids. A flow of 1 ml/min was used and 2 ml of sample flow was alternated with a flow of 2 mL of pure water as a reference. The toluene in water solution concentrations were calibrated using UV/Vis spectroscopy between 190 - 600 nm (Cary 50 Bio UV/Vis spectrophotometer), using quartz cuvettes with a path length of 1 cm filled with 1.5 mL of analyte solution.

In Fig. 13(A) we can appreciate the propagation loss induced by the mesoporous silica coating. From these spectra low losses between 6.4 to 6.7 µm are visible, which is in accordance with the performed simulations (see section 3). However, higher losses are visible between 6.7 to 6.85 µm and we attribute this absorption to the C-N vibration at 6.76 µm of CTAB template remaining in the coating after fabrication.

Optics EXPRESS

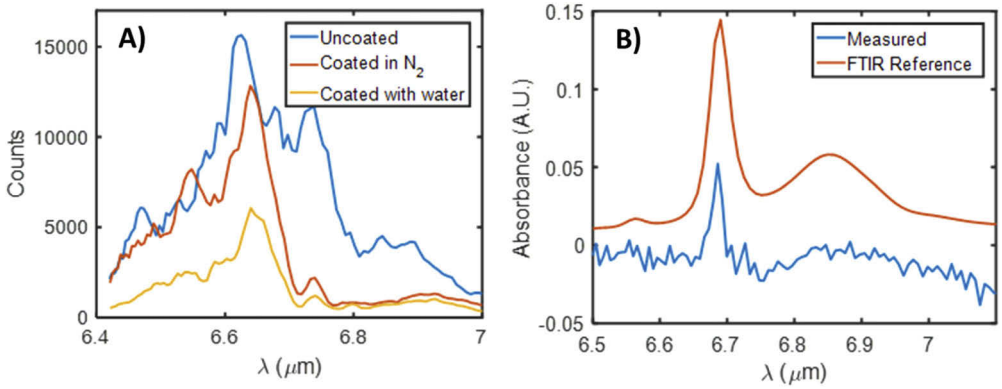


**Fig. 13.** (A) detected power spectrum of the uncoated sample and sample with coating with and without flowing water over the sensor surface; (B) measured absorbance spectrum for 133 ppm of toluene in water compared with the experimental FTIR reference spectrum.

Flowing water over the sensor resulted in an additional 2-6 dB power drop over the wavelength range of interest, as shown in Fig. 13(A). From simulations, the water on top of the coating is not the cause of this extra loss. Instead the origin can be attributed to a limited penetration of water in the coating, which has already been shown in previous work [22].

For the sensing of toluene in water we focused on the 6.5-7.0 μm wavelength range where the spectrally well separated skeleton ring vibrations of aromatic hydrocarbons are located. A representative measured absorbance spectrum obtained for the enrichment of a 133 ppm toluene in water solution into the mesoporous silica coating is shown in Fig. 13(B). It clearly indicates an absorption band at 6.686 μm (1496 $cm^{-1}$), which is in in very good agreement with the experimental reference spectrum obtained from Fourier Transform IR (FTIR) transmission measurements. Note that despite the high absorption at 6.76 μm, the second band of toluene could be reproduced.

Furthermore, successful and fast enrichment and hence response time of the sensing system for aqueous toluene solutions with concentrations ranging between 15 - 133 ppm are visible from the time profiles in Fig. 14(A), showing the response of the sensing system when applying the toluene in water solution (˜2 mins) and the recovery after changing back to pure water (~3 minutes). Note the delay of ~50s of the enrichment corresponds to the time required to exchange the dead volume in the flow system.

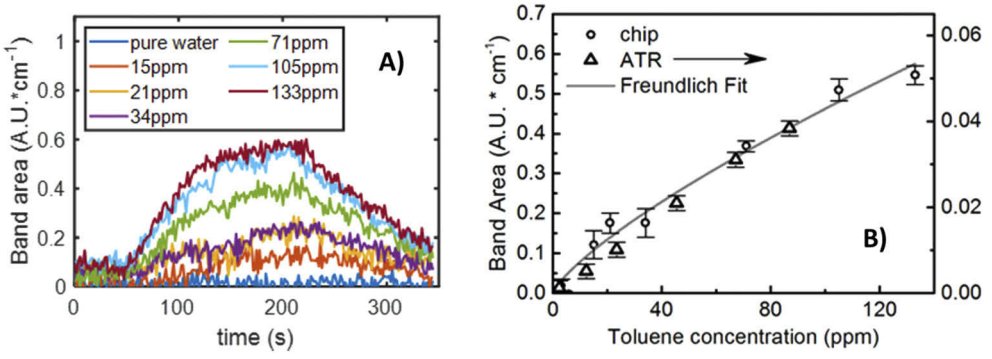


**Fig. 14.** (A) time response profiles of the system. (B) calibration function (Freundlich fit) for the enrichment of toluene in water for the chip system and ATR experiments.

Optics EXPRESS

For calibration, the band area between 1480 $cm^{-1}$ and 1510 $cm^{-1}$ was determined and the obtained data points (Fig. 14(B)) were fitted with the Freundlich equation [22,37]:

$$q_e = K_F c^{\frac{1}{n}}$$

with the amount of absorbed analyte $q_e$, the concentration of the analyte in the applied liquid c, the Freundlich affinity coefficient $K_F$ and a linearity index n. Here, $K_F = 0.0136$ and $n = 1.306$ were the obtained fitting parameters. The Freundlich equation serves as a calibration function and allows for retrieving the limit of detection (LOD) defined as $q_e(LOD) = 3\dot{c}\sigma$, with σ being the standard deviation of the noise level determined by 100% lines obtained from consecutively recorded spectra. The noise floor of the spectrometer developed in the AQUARIUS project left room for improvements resulting in a high noise level of 0.02 A.U. This corresponds to a LOD of 7 ppm. Using a state of the art EC-QCL with high power and low-noise emission, Schwaighofer et al. recently achieved an RMS noise level of $6{\cdot}10^{-5}$ A.U. [38]. Assuming this noise floor and a signal level of 0.06 A.U., as for the spectrum given in Fig. 12(A) LOD of 20 ppb would be possible.

Finally, we evaluated if the enrichment behavior of the mesoporous silica coating on the structured waveguide surface is similar to our previous results of one-layer coatings on planar ATR crystals [22]. To this end, toluene solutions were also applied to a Si ATR crystal coated with the same mesoporous silica coating and the thereby obtained band areas are given in Fig. 14(B). As in contrast to the discrete absorption spots found in ATR spectroscopy, the presented waveguide allows for higher effective interaction path lengths *d*. Here, the effective path lengths were calculated to be $d_{ATR}$=6.48 µm and $d_{chip}$=87.2 µm. $d_{chip}$ was calculated as product of the simulated confinement factor (1.09%) and the physical length of the waveguide of 8 mm. Note that the confinement factor and hence $d_{chip}$ was calculated using the BEMA model for the refractive index of the coating. Due to this difference in effective path lengths, the absorption bands obtained from ATR experiments are lower and therefore given on a different y-axis to show the similarity of the calibration functions for each setup. To compare both experimental setups numerically, the enrichment factor, defined as the ratio of the band area of adsorbed toluene in the mesoporous coating and the applied concentration in solution obtained from IR transmission measurements, was derived. For a concentration of 70 ppm toluene, enrichment factors for the ATR and chip experiments of 860 and 760 were obtained, respectively. Given the uncertainties in the actual effective path length of the chip (*e.g.* definition of the interaction volume by the O-ring) as well as the use of the BEMA model to retrieve the refractive index of the coating, this result is in excellent agreement and confirms that the multi-layer coating as well as the structured chip surface do not affect the enrichment capabilities of the mesoporous silica cladding.

## 6. Summary and conclusions

A Ge-based ATR-on-a-chip sensing platform operating in the 6.5-7.5 µm wavelength range and capable of sensing toluene in water was presented. The sensing chips consist of 1 µm etched trenched rib waveguides on a 2 µm germanium-on-silicon platform. Monolithically integrated microlenses on the back of the chip in combination with Au-coated grating couplers provide a broadband and tolerant optical interfacing allowing fast and easy chip replacement. The PICs are coated with a 3D hexagonal mesoporous silica coating which is organically modified to be hydrophobic and is capable of reversibly adsorbing and accumulating toluene. The sensing performance was evaluated with solutions of toluene in water (15–133 ppm) using a compact tunable laser mid-IR spectrometer. With a noise floor of 0.02 AU, a LOD of 7 ppm was determined. The adsorption and desorption capabilities of the coating were evaluated. While this paper focuses on the detection of toluene in water, the mesoporous coating can also be used to enhance other aromatic hydrocarbons [22]. With further improvements on the spectrometer to reduce the noise floor such as using a continuous-wave light source, reducing stray interference

Optics EXPRESS

and increasing the buffer/averaging depth, we expect to be able to reach sub-ppm LODs, making this a very attractive platform for the in-line sensing of organic contaminants in water.

## Funding

Horizon 2020 Framework Programme (731465).

## Acknowledgments

The authors acknowledge Delphine-Marris Morini, Aditya Malik and John Bowers for providing advice, SiGe wafers and samples during the early stages of the project. We also acknowledge Jindrich Windels for the design and fabrication of the custom parts in the in-house optical set-up

This work was carried out in the context of the AQUARIUS project, which has received funding from the European Union's Horizon 2020 research and innovation program under grant agreement No. 731465.

Portions of this work were presented at the OSA Optical Sensors and Sensing Congress in June 2020, Integrated Mid-IR Waveguide Sensor for Laser Based Trace Analysis in Aqueous Solutions

## Disclosures

The authors declare no conflicts of interest.

## References

1. C. Dettenrieder, Y. Raichlin, A. Katzir, and B. Mizaikoff, "Toward the Required Detection Limits for Volatile Organic Constituents in Marine Environments with Infrared Evanescent Field Chemical Sensors," Sensors **19**(17), 3644 (2019).
2. Luis Rodriguez-Saona, Huseyin Ayvaz, and Randy L. Wehling, "Infrared and Raman Spectroscopy," *Food Analysis* Springer, Cham, 2017. 107–127.
3. R. Lu, W. W. Li, B. Mizaikoff, A. Katzir, Y. Raichlin, G. P. Sheng, and H. Q. Yu, "High-sensitivity infrared attenuated total reflectance sensors for in situ multicomponent detection of volatile organic compounds in water," Nat. Protoc. **11**(2), 377–386 (2016).
4. Montreal Protocol, "Montreal protocol on substances that deplete the ozone layer," (US Government Printing Office 26, Washington, DC, 1987): 128–136.
5. ISO, EN. "9377 2, 2000. Water Quality-Determination of Hydrocarbon Oil Index-Part 2: Method Using Solvent Extraction and Gas Chromatography. Technical Committee ISO," German version, July (2001).
6. A. O. Adeniji, O. O. Okoh, and A. I. Okoh, "Analytical methods for the determination of the distribution of total petroleum hydrocarbons in the water and sediment of aquatic systems: A review," J. Chem. **2017**, 1–13 (2017).
7. L. Wagner, C. Kalli, E. O. Fridjonsson, E. F. May, J. Zhen, and M. L. Johns, "Simultaneous quantification of aliphatic and aromatic hydrocarbons in produced water analysis using mobile 1H NMR," Meas. Sci. Technol. **29**(8), 085501 (2018).
8. World Health Organization. "A global overview of national regulations and standards for drinking-water quality," (2018)
9. G. Z. Mashanovich, C. J. Mitchell, J. S. Penades, A. Z. Khokhar, C. G. Littlejohns, W. Cao, Z. Qu, S. Stanković, F. Y. Gardes, T. B. Masaud, and H. M. Chong, "Germanium mid-infrared photonic devices," J. Lightwave Technol. **35**(4), 624–630 (2017).
10. H. Lin, Z. Luo, T. Gu, L. C. Kimerling, K. Wada, A. Agarwal, and J. Hu, "Mid-infrared integrated photonics on silicon: a perspective," Nanophotonics **7**(2), 393–420 (2017).
11. U. Griškevičiūtė, R. W. Millar, K. Gallacher, L. Baldassarre, M. Sorel, M. Ortolani, and D. J. Paul, "Fingerprint mid-infrared sensing with germanium on silicon waveguides," In *2019 Conference on Lasers and Electro-Optics (CLEO)* 2019 May 5 (pp. 1–2). IEEE.
12. Q. Liu, J. M. Ramirez, V. Vakarin, X. Le Roux, A. Ballabio, J. Frigerio, D. Chrastina, G. Isella, D. Bouville, L. Vivien, and C. A. Ramos, "Mid-infrared sensing between 5.2 and 6.6 μm wavelengths using Ge-rich SiGe waveguides," Opt. Mater. Express **8**(5), 1305 (2018).
13. U. Griškevičiūtė, R. W. Millar, K. Gallacher, J. Valente, and D. J. Paul, "Ge-on-Si waveguides for sensing in the molecular fingerprint regime," Opt. Express **28**(4), 5749 (2020).
14. V. Mittal, M. Nedeljkovic, A. Z. Khokhar, L. G. Carpenter, G. S. Murugan, H. M. Chong, P. N. Bartlett, G. Z. Mashanovich, and J. S. Wilkinson, "Waveguide mid-infrared absorption spectroscopy of proteins in the spectral fingerprint region," In *Optics and the Brain* 2019 Apr 14 (pp. JT4A-30). Optical Society of America.
15. V. Mittal, M. Nedeljkovic, L. G. Carpenter, A. Z. Khokhar, H. M. Chong, G. Z. Mashanovich, P. N. Bartlett, and J. S. Wilkinson, "Waveguide absorption spectroscopy of bovine serum albumin in the mid-infrared fingerprint region," ACS Sens. **4**(7), 1749–1753 (2019).

Optics EXPRESS


16. Y. C. Chang, P. Wägli, V. Paeder, A. Homsy, L. Hvozdara, P. van der Wal, J. Di Francesco, N. F. de Rooij, and H. P. Herzig, "Cocaine detection by a mid-infrared waveguide integrated with a microfluidic chip," Lab Chip **12**(17), 3020 (2012).
17. P. Wägli, Y. C. Chang, A. Homsy, L. Hvozdara, H. P. Herzig, and N. F. de Rooij, "Microfluidic droplet-based liquid–liquid extraction and on-chip IR spectroscopy detection of cocaine in human saliva," Anal. Chem. **85**(15), 7558–7565 (2013).
18. D. Marris-Morini, V. Vakarin, J. M. Ramirez, Q. Liu, A. Ballabio, J. Frigerio, M. Montesinos, C. Alonso-Ramos, X. Le Roux, S. Serna, and D. Benedikovic, "Germanium-based integrated photonics from near-to mid-infrared applications," Nanophotonics **7**(11), 1781–1793 (2018).
19. G. Ramer and B. Lendl, Attenuated Total Reflection F ourier Transform Infrared Spectroscopy. Encyclopedia of Analytical Chemistry: Applications, Theory and Instrumentation. 2006 Sep 15.
20. E. Rosenberg, R. Krska, and R. Kellner, "Theoretical and practical response evaluation of a fiber optic sensor for chlorinated hydrocarbons in water," Fresenius' J. Anal. Chem. **348**(8-9), 560–562 (1994).
21. R. Göbel, R. Krska, R. Kellner, R. W. Seitz, and S. A. Tomellini, "Investigation of different polymers as coating materials for IR/ATR spectroscopic trace analysis of chlorinated hydrocarbons in water," Appl. Spectrosc. **48**(6), 678–683 (1994).
22. B. Baumgartner, J. Hayden, A. Schwaighofer, and B. Lendl, "In Situ IR Spectroscopy of Mesoporous Silica Films for Monitoring Adsorption Processes and Trace Analysis," ACS Appl. Nano Mater. **1**(12), 7083–7091 (2018).
23. B. Baumgartner, S. Freitag, C. Gasser, and B. Lendl, "A pocket-sized 3D-printed attenuated total reflection-infrared filtometer combined with functionalized silica films for nitrate sensing in water," Sens. Actuators, B **310**, 127847 (2020).
24. B. Baumgartner, J. Hayden, and B. Lendl, "Mesoporous silica films for sensing volatile organic compounds using attenuated total reflection spectroscopy," Sens. Actuators, B **302**, 127194 (2020).
25. N. Mangal, B. Snyder, J. Van Campenhout, G. Van Steenberge, and J. Missinne, "Expanded-Beam Backside Coupling Interface for Alignment-Tolerant Packaging of Silicon Photonics," IEEE J. Sel. Top. Quantum Electron. **26**(2), 1–7 (2020).
26. C. Scarcella, K. Gradkowski, L. Carroll, J. S. Lee, M. Duperron, D. Fowler, and P. O'Brien, "Pluggable single-mode fiber-array-to-PIC coupling using micro-lenses," IEEE Photonics Technol. Lett. **29**(22), 1943–1946 (2017).
27. N. Mangal, J. Missinne, J. Van Campenhout, G. Van Steenberge, and B. Snyder, "Through-substrate coupling elements for silicon-photonics-based short-reach optical interconnects," In Optical Interconnects XIX 2019 Mar 4 (Vol. 10924, p. 109240D). International Society for Optics and Photonics.
28. J. Missinne, N. Teigell Benéitez, N. Mangal, J. Zhang, A. Vasiliev, J. Van Campenhout, B. Snyder, G. Roelkens, and G. Van Steenberge, "Alignment-tolerant interfacing of a photonic integrated circuit using back side etched silicon microlenses," In Silicon Photonics XIV 2019 Mar 4 (Vol. 10923, p. 1092304). International Society for Optics and Photonics.
29. K. Gallacher, R. W. Millar, U. Griškevičiūte, L. Baldassarre, M. Sorel, M. Ortolani, and D. J. Paul, "Low loss Ge-on-Si waveguides operating in the 8–14 μm atmospheric transmission window," Opt. Express **26**(20), 25667 (2018).
30. A. Malik, M. Muneeb, S. Radosavljevic, M. Nedeljkovic, J. S. Penades, G. Mashanovich, Y. Shimura, G. Lepage, P. Verheyen, W. Vanherle, and T. Van Opstal, "Silicon-based photonic integrated circuits for the mid-infrared," Procedia Eng. **140**, 144–151 (2016).
31. S. Radosavljevic, B. Kuyken, and G. Roelkens, "Efficient 5.2 μm wavelength fiber-to-chip grating couplers for the Ge-on-Si and Ge-on-SOI mid-infrared waveguide platform," Opt. Express **25**(16), 19034 (2017).
32. C. Alonso-Ramos, M. Nedeljkovic, D. Benedikovic, J. S. Penadés, C. G. Littlejohns, A. Z. Khokhar, D. Pérez-Galacho, L. Vivien, P. Cheben, and G. Z. Mashanovich, "Germanium-on-silicon mid-infrared grating couplers with low-reflectivity inverse taper excitation," Opt. Lett. **41**(18), 4324 (2016).
33. G. A. Niklasson, C. G. Granqvist, and O. Hunderi, "Effective medium models for the optical properties of inhomogeneous materials," Appl. Opt. **20**(1), 26 (1981).
34. B. Baumgartner, J. Hayden, J. Loizillon, S. Steinbacher, D. Grosso, and B. Lendl, "Pore size-dependent structure of confined water in mesoporous silica films from water adsorption/desorption using ATR–FTIR spectroscopy," Langmuir **35**(37), 11986–11994 (2019).
35. J. Troles, Q. Coulombier, G. Canat, M. Duhant, W. Renard, P. Toupin, L. Calvez, G. Renversez, F. Smektala, M. El Amraoui, and J. L. Adam, "Low loss microstructured chalcogenide fibers for large non linear effects at 1995nm," Opt. Express **18**(25), 26647 (2010).
36. J. M. Kriesel, N. Gat, B. E. Bernacki, R. L. Erikson, B. D. Cannon, T. L. Myers, C. M. Bledt, and J. A. Harrington, "Hollow core fiber optics for mid-wave and long-wave infrared spectroscopy," In Chemical, Biological, Radiological, Nuclear, and Explosives (CBRNE) Sensing XII 2011 Jun 3 (Vol. 8018, p. 80180 V). International Society for Optics and Photonics.
37. Y. S. Ho, "Selection of optimum sorption isotherm," Carbon **42**(10), 2115–2116 (2004).
38. A. Schwaighofer, M. Montemurro, S. Freitag, C. Kristament, M. J. Culzoni, and B. Lendl, "Beyond Fourier Transform Infrared Spectroscopy: External cavity quantum cascade laser-based mid-infrared transmission spectroscopy of proteins in the Amide I and Amide II Region," Anal. Chem. **90**(11), 7072–7079 (2018).